Journal of Power Sources 246 (2014) 213–218

Contents lists available at ScienceDirect

Journal of Power Sources

journal homepage: www.elsevier.com/locate/jpowsour

Microemulsion-assisted synthesis of ultrafine $Li_4Ti_5O_{12}$/C nanocomposite with oleic acid as carbon precursor and particle size controller

Yuan Wang [a], Haibo Rong [a], Benzhen Li [a], Lidan Xing [a,b,c], Xiaoping Li [a,b,c], Weishan Li [a,b,c,*]

[a] School of Chemistry and Environment, South China Normal University, Guangzhou 510006, China
[b] Key Laboratory of Electrochemical Technology on Energy Storage and Power Generation of Guangdong Higher Education Institutes, South China Normal University, Guangzhou 510006, China
[c] Engineering Research Center of Materials and Technology for Electrochemical Energy Storage (Ministry of Education), South China Normal University, Guangzhou 510006, China

HIGHLIGHTS

- Ultrafine $Li_4Ti_5O_{12}$/C composite was prepared by microemulsion-assisted method.
- Oleic acid was used as carbon precursor and particle size controller.
- Ultrafine $Li_4Ti_5O_{12}$ particles are uniformly dispersed in carbon matrix.
- The composite exhibits excellent rate performance and cyclic stability.

ARTICLE INFO

Article history:
Received 27 May 2013
Received in revised form
6 July 2013
Accepted 26 July 2013
Available online 2 August 2013

Keywords:
Lithium ion battery
Anode
Lithium titanate
Oleic acid
Carbon
Nanocomposite

ABSTRACT

Ultrafine $Li_4Ti_5O_{12}$/C composite is synthesized by microemulsion with oleic acid as carbon precursor and particle size controller. The as-prepared sample is characterized with X-ray diffraction (XRD), field emission scanning electron microscope (FE-SEM), transmission electron microscopy (TEM), thermogravimetry analysis (TGA) and nitrogen absorption–desorption isotherms, and its performance as anode of lithium ion battery is determined with charge–discharge test and electrochemical impedance spectroscopy (EIS). The characterizations show that the as-prepared sample is composed of ultrafine $Li_4Ti_5O_{12}$ particles with average size of 25 nm, which are uniformly dispersed in carbon matrix with a carbon content as low as 2.69 wt%. Charge–discharge test indicates that the as-prepared sample exhibits excellent rate performance and cycling stability. At 10C, the highest discharge capacity reaches 136.3 mAh g^{-1} and the capacity retention is 96.4% after 100 cycles. The improved performance of the $Li_4Ti_5O_{12}$/C composite is attributed to the ultrafine particle size and the uniform composite of $Li_4Ti_5O_{12}$ with carbon.

1. Introduction

Lithium ion battery (LIB) as an energy storage device has been attracting more and more attentions due to its high energy density [1–5]. Currently commercial LIB usually uses graphite as anode, but its low lithium-inserted potential and the changeable distance between layers of graphite affect the cyclic stability of LIB. Titanium dioxide (TiO_2), a widely used photocatalyst [6,7], is now being introduced as anode of LIB due to its higher lithium-inserted potential and structure stability [8–13]. However, the poor rate performance of TiO_2 cannot meet the demand of high power density of LIB [14–16].

Lithium titanate ($Li_4Ti_5O_{12}$, LTO), a composite of TiO_2 and Li_2O, is a promising anode material because of its superior performance to TiO_2 [17–20]. $Li_4Ti_5O_{12}$ has a spinel structure with space group of $Fd\bar{3}m$ and a transformation between a spinel structure of $Li_4Ti_5O_{12}$ and an ordered rock-salt structure of $Li_7Ti_5O_{12}$ through a two-phase equilibrium reaction during the lithium insertion and extraction processes [21–23], revealing a voltage plateau of ca. 1.55 V (vs. Li^+/Li) in the charge and discharge voltage profiles which is higher than graphite but lower than TiO_2 [24–26]. Besides, the lattice parameters

* Corresponding author. School of Chemistry and Environment, South China Normal University, Guangzhou 510006, China. Tel./fax: +86 20 39310256.
E-mail address: liwsh@scnu.edu.cn (W. Li).

0378-7753/$ – see front matter © 2013 Elsevier B.V. All rights reserved.
http://dx.doi.org/10.1016/j.jpowsour.2013.07.093

between $Li_4Ti_5O_{12}$ and $Li_7Ti_5O_{12}$ are very similar with the difference less than 0.1% [27,28]. The minimal lattice change of $Li_4Ti_5O_{12}$ gives rise to an exceptional sturdy rigid skeleton structure which tolerates long-term insertion and extraction reaction of lithium. Furthermore, $Li_4Ti_5O_{12}$ has a high thermodynamic stability [17]. However, the rate performance of $Li_4Ti_5O_{12}$ needs to be improved because its conductivity is low ($<10^{-13}$ S cm^{-1}) [29,30].

To improve the rate performance of $Li_4Ti_5O_{12}$, three strategies have been proposed. The first is to reduce the particle size. Nano-particles provide short diffusion pathway of Li^+ and improve the utilization of active materials [31–34]. However, due to the larger specific surface area, the nanoparticles tend to be agglomerated. The second is to introduce electronically conductive phase such as carbon, metal or metal oxide [35–37]. The conductive materials improve the electrical contact between the active materials, but reduce the specific capacity of the electrode. The third is to dope with foreign ions, such as Zn^{2+} [38], La^{3+} [39], Al^{3+} [40], Zr^{4+} [41], V^{5+} [42], Nb^{5+} [43], Mo^{6+} [44], and Br^- [45]. The doping changes the energy level distribution, but the improvement in conductivity is not significant.

Microemulsion method has been widely used to synthesize various nanoscale crystallines in the last several decades, since it is a powerful approach to control the particle size and particle distribution [46–49]. In this work, we used microemulsion method to develop a novel anode material, ultrafine $Li_4Ti_5O_{12}$/C composite with low carbon content, which combines the advantages of nanoparticle and carbon introduction and avoids their shortages. In the preparation of this composite, microemulsion method was used for the formation of nanoparticles and oleic acid was introduced as carbon precursor and particle size controller. The performance of the composite as anode of lithium ion battery was investigated.

2. Experimental section

2.1. Material preparation

All the chemicals were used as received without further purification.

2.1.1. Preparation of titanium dioxide

A certain amount of cetyl trimethyl ammonium bromide (CTAB) was added into 150 ml deionized water, suffering from ultrasonic and mechanical stirring, a milky solution was obtained and marked as solution A. Titanium isopropoxide (TTIP) and oleic acid with mole ratio of 1:0.06 were dissolved into 60 ml *n*-hexane, then solution B was derived after magnetic stirring for 0.5 h. The solution B was added to solution A dropwise and the mixture was stirred for 1 h at room temperature. The concentration of Ti^{4+} is 0.13 mol L^{-1} and the mole ratio of TTIP and CTAB is 1:1.17. The yellowish precipitate was collected by filtrating and washing several times with deionized water and then drying at 80 °C to obtain titanium dioxide (TiO_2).

2.1.2. Preparation of $Li_4Ti_5O_{12}$/C nanocomposite

The as-prepared TiO_2 was thoroughly mixed with lithium carbonate (Li_2CO_3) with n(Li):n(Ti) = 0.85 and the mixture were firstly annealed at 400 °C for 2 h under argon atmosphere. Then after undergoing regrinding, the powders were further calcinated at 800 °C for 12 h to get the final product, marked as MAM-LTO/C. For comparison, the bulk $Li_4Ti_5O_{12}$ powders were also synthesized by one step solid state method with TiO_2 (Aladdin) and Li_2CO_3 as raw materials under identical reaction conditions and the resultant material was marked as SSM-LTO.

2.2. Cell assembly

The electrochemical tests were performed in coin-type cell (CR2025) based on the configuration of Li/electrolyte/$Li_4Ti_5O_{12}$. Li electrode was a lithium metal foil. $Li_4Ti_5O_{12}$ electrode was prepared as follows. The as-prepared active material, acetylene black and polyvinylidene fluoride (PVDF) were mixed in a weight ratio of 80:10:10 and then dispersed in *N*-Methyl pyrrolidone (NMP) solvent to form homogeneous slurry. The slurry was coated on copper foil current collector and dried at 120 °C for 12 h under vacuum condition. Then the electrode was cut into square with the area of 1×1 cm^2 for the cell assembly. The electrolyte was 1 mol L^{-1} $LiPF_6$ in a 1:1 (w/w) mixture of ethylene carbonate (EC) and dimethyl carbonate (DMC). Celgard 2300 microporous membrane was used as the separator. The cells assembly was performed in a glove box filled with high purity argon.

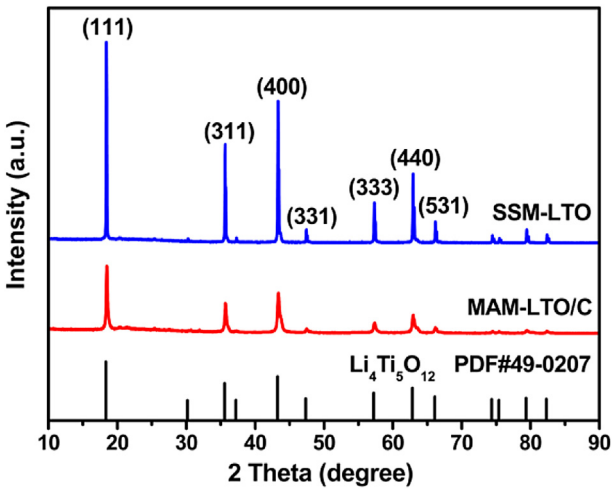

Fig. 1. Wide-angle powder XRD patterns of MAM-LTO/C and SSM-LTO. The standard card of $Li_4Ti_5O_{12}$ is also included.

2.3. Material characterization

The crystalline phase information of the as-prepared materials was obtained by a powder X-ray diffraction (XRD; Bruker D8 Advance, Germany) with a Cu Kα radiation. The diffraction patterns were recorded at room temperature in the 2θ range from 10° to 90° with a scanning step of 5° min^{-1}. The surface morphology of the powders was observed by a field emission scanning electron microscope (FE-SEM; ZEISS Ultra 55, Germany) and transmission electron microscope (TEM; JEM-2100HR, USA). The carbon content

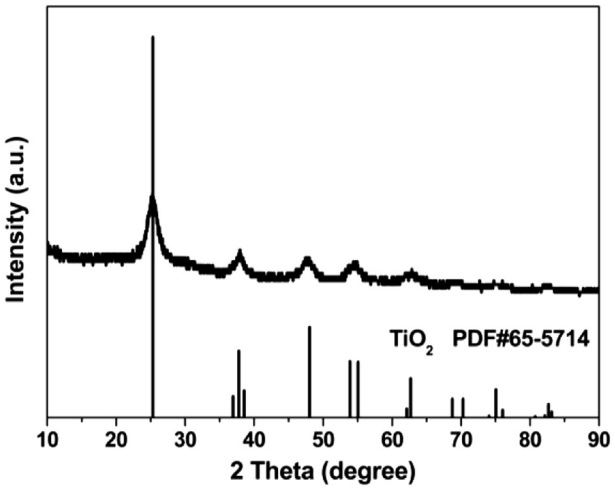

Fig. 2. Wide-angle powder XRD pattern of precursor (amorphous TiO_2).

of the yielded $Li_4Ti_5O_{12}$/C nanocomposite was determined by a TG analyzer (NETZSCH STA 409PC) with a heating rate of 10 °C min^{-1} from room temperature to 800 °C under air atmosphere. The nitrogen absorption–desorption isotherms were determined using a Micromeritics ASAP 2020-physisorption analyzer (USA).

Constant current charge–discharge tests were performed on a multi-channel battery test system (LAND CT2001A, China) with a voltage window of 1–2.5 V (vs. Li^+/Li) at constant temperature of 25 °C. Electrochemical impedance spectroscopy (EIS) was conducted in an Autolab (PGSTAT-302N, Eco Echemie B.V. Company) at open circuit voltage with the frequency range from 10^{-2} to 10^6 Hz. In the EIS measurement, Li anode was used as both the counter electrode and the reference electrode and $Li_4Ti_5O_{12}$ electrode was used as the working electrode.

3. Results and discussion

Fig. 1 shows the XRD patterns of MAM-LTO/C and SSM-LTO. The diffraction peaks of two samples are indexed to spinel $Li_4Ti_5O_{12}$ (PDF#49-0207) and no significant impurity peaks are detected, indicating that pure spinel $Li_4Ti_5O_{12}$ materials are obtained. The intensity of diffraction peaks is much stronger for SSM-LTO than MAM-LTO/C and the width of the half peaks are smaller for SSM-LTO than MAM-LTO/C, suggesting that MAM-LTO/C has less crystalline but a smaller particle size. The XRD pattern of the precursor (as-prepared TiO_2) is also obtained (Fig. 2.). It is found that the diffraction peaks of the precursor are consistent with the standard card of TiO_2 (PDF#65-5714). The blunt peaks indicate that the precursor is amorphous TiO_2.

The surface morphology and the microstructure of the materials are detected by FE-SEM and TEM, as shown in Fig. 3. Comparing Fig. 3(a) with Fig. 3(b), it can be found that the particle size is smaller and more uniform for the MAM-LTO/C. The average particle size is further identified by TEM images, which is 260 nm for SSM-LTO (Fig. 3(c)) and 25 nm for MAM-LTO/C (Fig. 3(d)). It can be seen from Fig. 3(d) that $Li_4Ti_5O_{12}$ nanoparticles in MAM-LTO/C are uniformly dispersed in carbon matrix. Therefore, with our oil-in-water system, $Li_4Ti_5O_{12}$/C nanocomposite with ultrafine $Li_4Ti_5O_{12}$

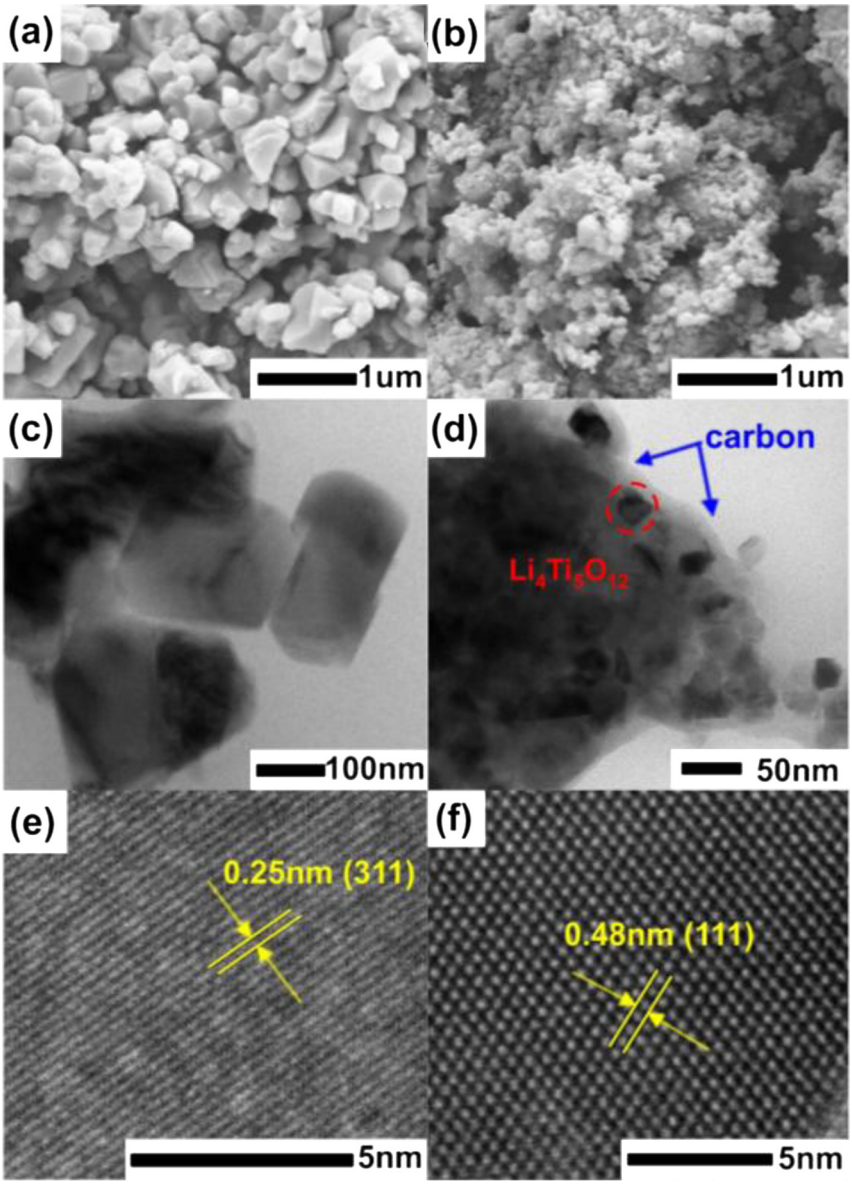

Fig. 3. SEM, TEM and HR-TEM images of SSM-LTO (a, c and e) and MAM-LTO/C (b, d and f).

particles uniformly dispersed in carbon is successfully obtained. Fig. 3(e) and (f) is the high-resolution TEM (HR-TEM) images of SSM-LTO and MAM-LTO/C. The d-spacing is 0.25 nm for SSM-LTO and 0.48 nm for MAM-LTO/C, corresponding to the (311) plane and the (111) plane of $Li_4Ti_5O_{12}$, respectively. The TEM image for the precursor (amorphous TiO_2) is also obtained, as shown in Fig. 4. It is found that the TiO_2 particles are almost monodispersed, with particle size of 3 ~ 5 nm, signifying that the microemulsion-assisted method is effective in synthesizing ultrafine nano-materials.

The carbon content of MAM-LTO/C nanocomposite is evaluated by TGA. Fig. 5 presents the TG profiles of the MAM-LTO/C and SSM-LTO. It can be seen from Fig. 5 that there is a slight weight loss before 80 °C for two samples, which can be attributed to the evaporation of trace absorbed water. No significant weight loss can be observed for SSM-LTO before 600 °C. Comparatively, there is a weight loss for MAM-LTO/C, which should be ascribed to the decomposition of carbon. The carbon content estimated from this weight loss is 2.69% for MAM-LTO/C. With the further increase of the temperature (>600 °C), both samples show a similar weight loss, which can be attributed to volatilization of Li_2O.

The formation process of $Li_4Ti_5O_{12}$/C nanocomposite is presented schematically in Fig. 6. Microemulsion is formed when *n*-hexane solution containing TTIP and oleic acid is dropwise added into aqueous solution under violent stirring and functions as a micro-reactor for the formation of TiO_2. Once TiO_2 is formed from the hydrolysis of TTIP, oleic acid is absorbed onto the surface and prevents the further growth of TiO_2 nuclei. CTAB functions as a stabilizer by distributing on the oil–water surface to prevent the microemulsion from aggregation. Furthermore, oleic acid remains in the sample to protect the nanoparticles from agglomeration till calcination at which it is transformed into carbon.

Fig. 7 illustrates the charge–discharge profiles of two samples under different current rates. Ten cycles are conducted at each rate and the profiles are extracted from the fifth charge/discharge cycle for each rate. It can be seen from Fig. 7 that MAM-LTO/C exhibits much better charge–discharge performance than SSM-LTO, especially at high rates. At 15C, the discharge capacity is 118.4 mAh g^{-1} for MAM-LTO/C, but only 26.3 mAh g^{-1} for SSM-LTO. The significant difference in rate performance between MAM-LTO/C and SSM-LTO indicates the contributions of ultrafine particles and uniform carbon composite. It can be noted that at lower rates (0.1C, 0.5C and

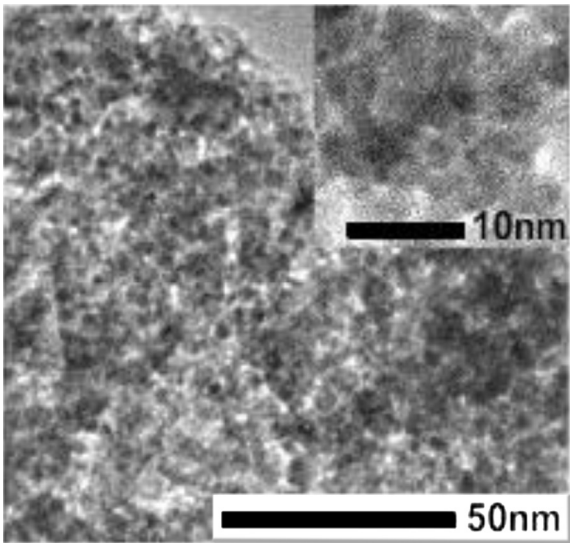

Fig. 4. TEM image of precursor (amorphous TiO_2) and the inset is the magnification image.

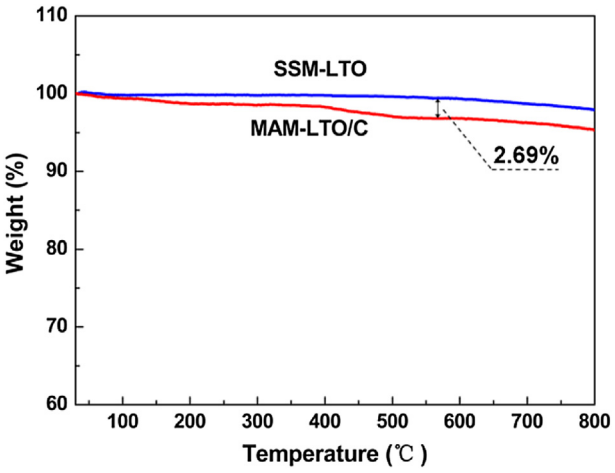

Fig. 5. TG profiles of the MAM-LTO/C and SSM-LTO.

1C), the charge and discharge capacities of MAM-LTO/C nanocomposite surpass the theoretical value of pure spinel $Li_4Ti_5O_{12}$ (175 mAh g^{-1}). The similar phenomena have also been observed by other groups [50–54]. This is characteristic of nano $Li_4Ti_5O_{12}$ materials. The larger surface area of nanoparticles contributes to partial capacity due to the surface lithium storage [55–57].

The surface area of two samples are determined by the nitrogen absorption–desorption isotherms, as shown in Fig. 8. As can be seen, the two samples display typical type-IV isotherm with distinct hysteresis loops at high pressures. The insets are the pore size distribution of materials. There is a narrow peak at about 3.8 nm and a broad peak centered at ca. 7 nm for MAM-LTO/C (Fig. 8(a)), indicating the presence of mesopores and macropores, which can be ascribed to the gaps between nanoparticles and carbon matrix. Differently, only a broad peak centered at ca. 60 nm can be observed for SSM-LTO (Fig. 8(b)), which is formed by the agglomerated particles. The BET surface area is 19.69 m^2 g^{-1} for MAM-LTO/C and 2.90 m^2 g^{-1} for SSM-LTO, respectively, confirming the contribution of nanoparticles in MAM-LTO/C to the specific surface area.

Electrochemical impedance spectroscopy is used to further understand the difference in rate performance between MAM-LTO/C and SSM-LTO. Fig. 9 presents the Nyquist plots of two samples at open circuit voltage, which includes a semicircle at high frequencies and a straight line at low frequencies. The diameter of the semicircle

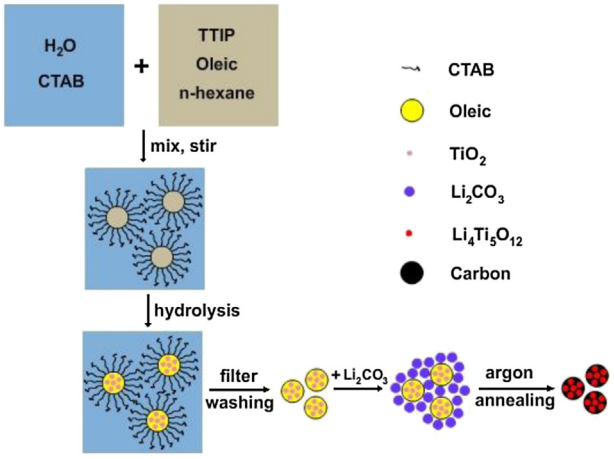

Fig. 6. Schematic formation process of $Li_4Ti_5O_{12}$/C nanocomposite.

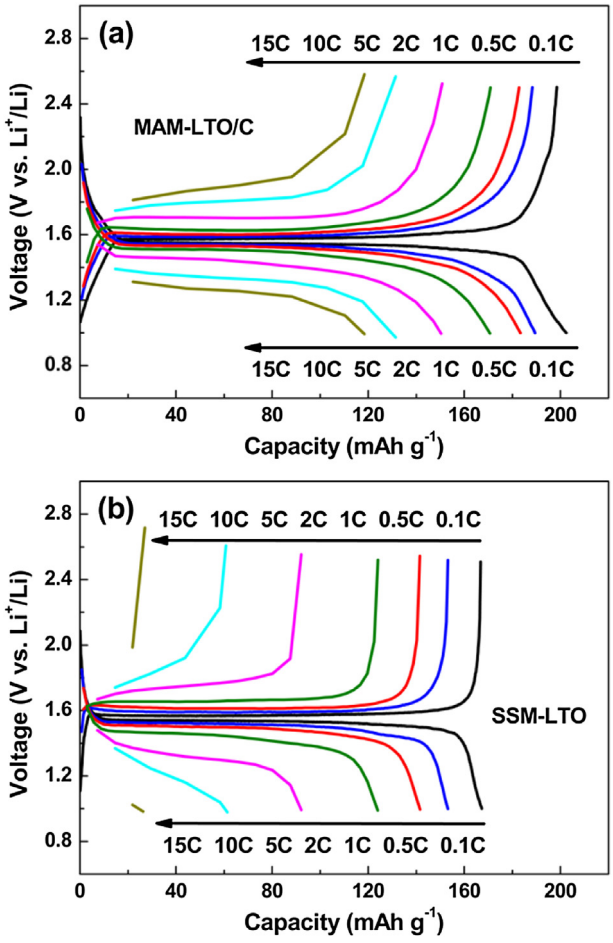

Fig. 7. Charge–discharge profiles of MAM-LTO/C (a) and SSM-LTO (b) at different current rates.

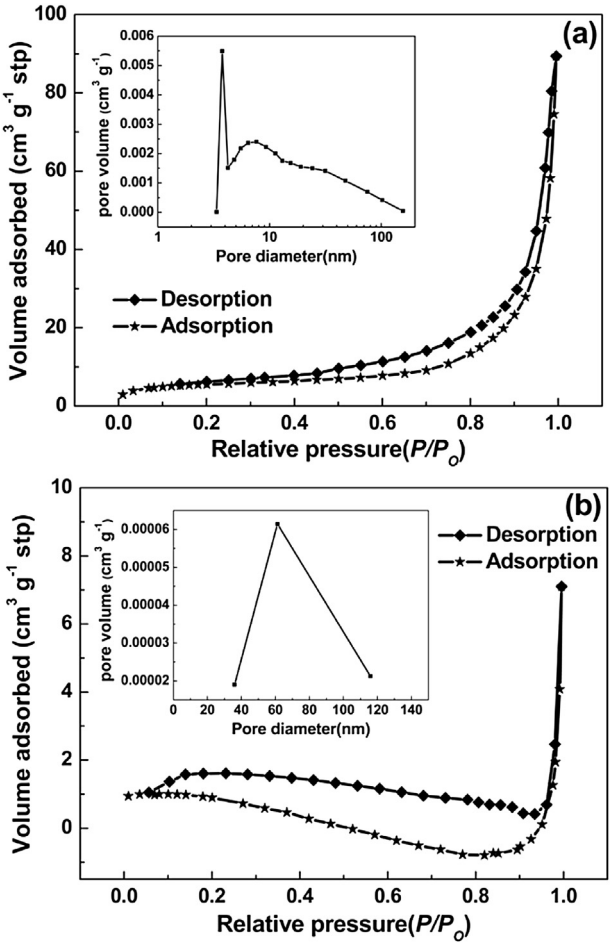

Fig. 8. Nitrogen absorption–desorption isotherms for (a) MAM-LTO/C nanocomposite and (b) SSM-LTO. The insets show the pore size distribution of the materials.

reflects the charge transfer resistance (R_{ct}), while the slope of the straight line is related to the diffusion of lithium ion in the electrode materials. The diffusion coefficient of lithium ion (D_{Li}) is proportional to the slope of the straight line at low frequencies [58].

Apparently, the R_{ct} is much smaller and the slope of straight line is larger for MAM-LTO/C than those for SSM-LTO. Therefore, the nanoparticles uniformly dispersed in carbon matrix provide the composite with fast lithium insertion/de-insertion kinetics, resulting in the excellent rate performance of MAM-LTO/C.

High rate performance of battery materials is usually accompanied with a poor cyclic stability. The cyclic stability of the as-prepared samples is examined with high current rates. Fig. 10 compares the cyclic stability between MAM-LTO/C and SSM-LTO at charge–discharge rates of 5C and 10C. The cells are charged and discharged for three cycles at 0.1C before performing a long-term cycle at higher C-rates. It can be seen from Fig. 10 that two samples exhibit a capacity loss when they experience a change from low-current to high-current rate, which reflects the lower utilization of the active materials and can be ascribed to the larger polarization under higher current rate. The smaller capacity loss of MAM-LTO/C shows its lower polarization than SSM-LTO. For the 5C-rate (Fig. 10(a)), MAM-LTO/C delivers an initial discharge capacity of 161.3 mAh g^{-1}, achieves its maximum of 170.6 mAh g^{-1} at the 7th cycle and remains 163.3 mAh g^{-1} after 100 cycles with its capacity retention of 95.7%. The corresponding values for SSM-LTO are 99.4 mAh g^{-1}, 106.0 mAh g^{-1} (20th), 100.4 mAh g^{-1} and 94.7%, respectively. There is no significant difference in cyclic stability between two samples, although their capacities are different. Similar results can be observed for a higher C-rate (10C), as shown in Fig. 10(b). It is obvious that the ultrafine particles in MAM-LTO/C do not reduce its cyclic stability.

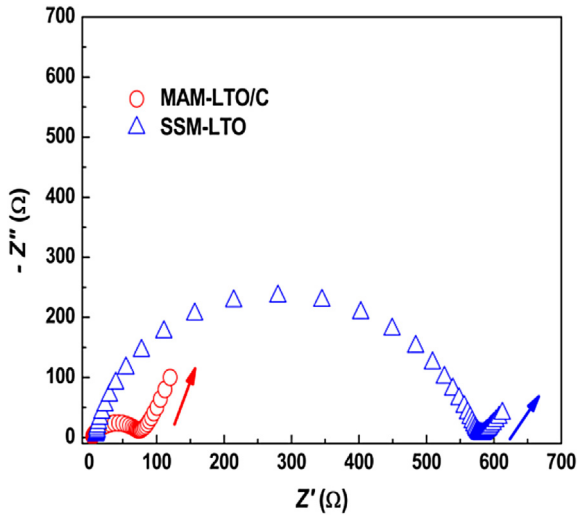

Fig. 9. Nyquist plots of cells after three charge/discharge cycles between 1.0 and 2.5 V (vs. Li^+/Li) at the charge–discharge rate of 0.1C.

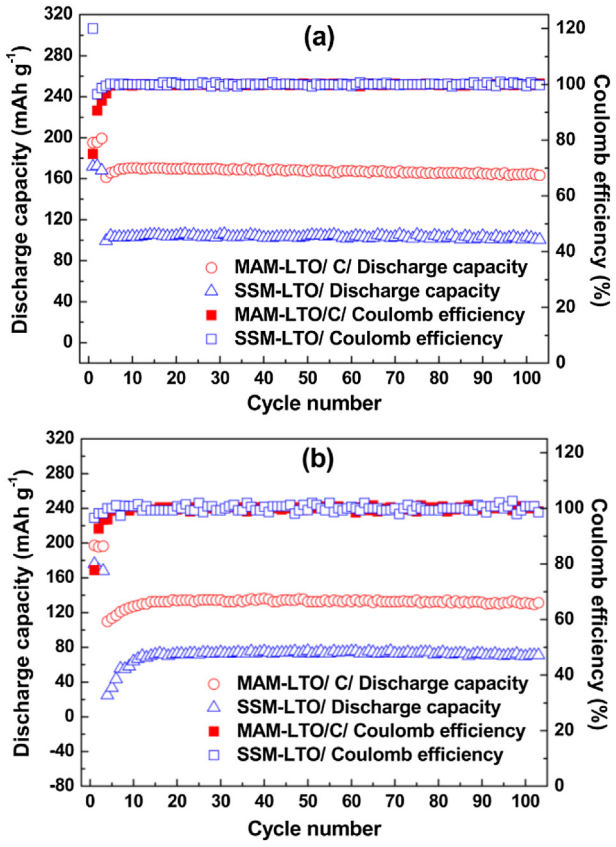

Fig. 10. Cycling performances of MAM-LTO/C and SSM-LTO at the charge–discharge rates of (a) 5C (b) 10C in the voltage windows of 1.0–2.5 V (vs. Li^+/Li).

4. Conclusions

In this paper, we reported a novel $Li_4Ti_5O_{12}$/C composite as anode of lithium ion battery. This composite was prepared by micro-emulsion method, in which oleic acid was introduced as carbon precursor and particle size controller and thus nanoparticles of $Li_4Ti_5O_{12}$ can be formed and uniformly dispersed in carbon. Charge–discharge test demonstrates that the resulting $Li_4Ti_5O_{12}$/C composite delivers excellent charge and discharge capacities with superior rate and cyclic performance. This performance can be ascribed to ultrafine $Li_4Ti_5O_{12}$ particles that are uniformly dispersed in carbon matrix.

Acknowledgments

This work was supported by the joint project of National Natural Science Foundation of China and Natural Science Foundation of Guangdong Province (Grant No. U1134002), Natural Science Fund of Guangdong Province (Grant No. 10351063101000001) and the joint project of Guangdong Province and Ministry of Education for the Cooperation among Industries, Universities and Institutes (Grant No. 2011B090400627).

References

[1] M.S. Dresselhaus, I.S. Thomas, Nature 414 (2001) 332–337.
[2] Y. Wang, H. Xia, L. Lu, J.Y. Lin, ACS Nano 4 (2010) 1425–1432.
[3] B. Scrosati, J. Garche, J. Power Sources 195 (2010) 2419–2430.
[4] F. Croce, M.L. Focarete, J. Hassoun, I. Meschini, B. Scrosati, Energy Environ. Sci. 4 (2011) 921–927.
[5] Y.J. Li, L. Hong, J.Q. Sun, F. Wu, S. Chen, Electrochim. Acta 85 (2012) 110–115.
[6] J.F. Lei, X.P. Li, W.S. Li, F.Q. Sun, D.S. Lu, Y.L. Lin, J. Solid State Electrochem. 16 (2012) 625–632.
[7] J.F. Lei, X.P. Li, W.S. Li, F.Q. Sun, D.S. Lu, J. Yi, Int. J. Hydrogen Energy 14 (2011) 8167–8172.
[8] A.R. Armstrong, G. Armstrong, J. Canales, R. García, P.G. Bruce, Adv. Mater. 17 (2005) 862–865.
[9] J. Yi, C.L. Tan, W.S. Li, J.F. Lei, L.S. Hao, Rare Metals 29 (2010) 505–510.
[10] J.F. Lei, W.S. Li, X.P. Li, E.J. Caims, J. Mater. Chem. 22 (2012) 22022–22027.
[11] J. Wang, Y.K. Zhou, Y.Y. Hu, R. O'Hayre, Z.P. Shao, J. Phys. Chem. C 115 (2011) 2529–2536.
[12] J. Yi, D.S. Lu, X.P. Li, W.S. Li, S.J. Hu, J.F. Lei, Y. Wang, J. Solid State Electrochem. 16 (2012) 443–448.
[13] J. Yi, X.P. Li, S.J. Hu, W.S. Li, R.H. Zeng, Z. Fu, L. Chen, Rare Metals 30 (2011) 589–594.
[14] M.G. Choi, Y.G. Lee, S.W. Song, K.M. Kim, Electrochim. Acta 55 (2010) 5975–5983.
[15] H.Q. Li, S.K. Martha, R.R. Unocic, H.M. Luo, S. Dai, J. Qu, J. Power Sources 218 (2012) 88–92.
[16] J.W. Zhang, X.X. Yan, J.W. Zhang, W. Cai, Z.S. Wu, Z.J. Zhang, J. Power Sources 198 (2012) 223–228.
[17] T.F. Yi, Y. Xie, Y.R. Zhu, R.S. Zhu, H.Y. Shen, J. Power Sources 222 (2012) 448–454.
[18] G.N. Zhu, H.J. Liu, J.H. Zhang, C.X. Wang, Y.G. Wang, Y.Y. Xia, Energy Environ. Sci. 4 (2011) 4016–4022.
[19] Z.N. Wan, R. Cai, S.M. Jiang, Z.P. Shao, J. Mater. Chem. 22 (2012) 17773–17781.
[20] G.J. Wang, J. Gao, L.J. Fu, N.H. Zhao, Y.P. Wu, T. Takamura, J. Power Sources 174 (2007) 1109–1112.
[21] M. Kitta, T. Akita, Y. Maeda, M. Kohyama, Langmuir 28 (2012) 12384–12392.
[22] I. Leonidov, O. Leonidova, L. Perelyaeva, R. Samigullina, S. Kovyazina, M. Patrakeev, Phys. Solid State 45 (2003) 2183–2188.
[23] A. Jaiswal, C.R. Horne, O. Chang, W. Zhang, W. Kong, E. Wang, T. Chern, M.M. Doeff, J. Electrochem. Soc. 156 (2009) A1041–A1046.
[24] L.F. Shen, H.S. Li, E. Uchaker, X.G. Zhang, G.Z. Cao, Nano. Lett. 12 (2012) 5673–5678.
[25] S. Komaba, N. Yabuuchi, T. Ozeki, K. Okushi, H. Yui, K. Konno, Y. Katayama, T. Miura, J. Power Sources 195 (2010) 6069–6074.
[26] P. Kubiak, T. Fröschl, N. Hüsing, U. Hörmann, U. Kaiser, R. Schiller, C.K. Weiss, K. Landfester, M.W. Mehrens, Small 7 (2011) 1690–1696.
[27] S. Ganapathy, M. Wagemaker, ACS Nano 6 (2012) 8702–8712.
[28] L.F. Shen, C.Z. Yuan, H.J. Luo, X.G. Zhang, K. Xu, Y.Y. Xia, J. Mater. Chem. 20 (2010) 6998–7004.
[29] J. Gao, C. Jiang, J. Ying, C. Wan, J. Power Sources 155 (2006) 364–367.
[30] Y.J. Bai, C. Gong, Y.X. Qi, N. Lun, J. Feng, J. Mater. Chem. 22 (2012) 19054–19060.
[31] A.S. Prakash, P. Manikandan, K. Ramesha, M. Sathiya, J.-M. Tarascon, A.K. Shukla, Chem. Mater. 22 (2010) 2857–2863.
[32] S.H. Yu, A. Pucci, T. Herntrich, M.G. Willinger, S.H. Baek, Y.E. Sung, N. Pinna, J. Mater. Chem. 26 (2011) 806–810.
[33] C.C. Li, Q.H. Li, L.B. Chen, T.H. Wang, ACS Appl. Mater. Interfaces 4 (2012) 1233–1238.
[34] J. Lim, E. Choi, V. Mathew, D. Kim, D. Ahn, J. Gim, S.H. Kang, J. Kim, J. Electrochem. Soc. 158 (2011) A275–A280.
[35] X.B. Hu, Z.J. Lin, K.R. Yang, Y.J. Huai, Z.H. Deng, Electrochim. Acta 56 (2011) 5046–5053.
[36] J.P. Zhu, W. Zu, J.J. Zhao, G. Yang, Q.B. Xu, J. Nanosci. Nanotechnol. 12 (2012) 2539–2542.
[37] S.H. Huang, Z.Y. Wen, X.J. Zhu, X.L. Yang, J. Electrochem. Soc. 152 (2005) A1301–A1305.
[38] T.F. Yi, H.P. Liu, Y.R. Zhu, L.J. Jiang, Y. Xie, R.S. Zhu, J. Power Sources 215 (2012) 258–265.
[39] J. Gao, C.Y. Jiang, C.R. Wan, J. Electrochem. Soc. 157 (2010) K39–K42.
[40] H.L. Zhao, Y. Li, Z.M. Zhu, J. Lin, Z.H. Tian, R.L. Wang, Electrochim. Acta 53 (2008) 7079–7083.
[41] X. Li, M.Z. Qu, Z.L. Yu, J. Alloys Compd. 487 (2009) L12–L17.
[42] Z.J. Yu, X.F. Zhang, G.L. Yang, J. Liu, J.W. Wang, R.S. Wang, J.P. Zhang, Electrochim. Acta 56 (2011) 8611–8617.
[43] T.F. Yi, Y. Xie, J. Shu, Z.H. Wang, C.B. Yue, R.S. Zhu, H.B. Qiao, J. Electrochem. Soc. 158 (2011) A266–A274.
[44] T.F. Yi, Y. Xie, L.J. Jiang, J. Shu, C.B. Yue, A.N. Zhou, M.F. Ye, RSC Adv. 2 (2012) 3541–3547.
[45] G.D. Du, N. Sharma, V.K. Peterson, J.A. Kimpton, D.Z. Jia, Z.P. Guo, Adv. Funct. Mater. 21 (2011) 3990–3997.
[46] L. Yang, R.S. Xie, L.Y. Liu, D.Q. Xiao, J.G. Zhu, J. Phys. Chem. C 115 (2011) 19507–19512.
[47] L.R. Li, M.H. Huang, J.J. Liu, Y.L. Guo, J. Power Sources 196 (2011) 1090–1096.
[48] C. Tiseanu, V.I. Parvulescu, M. Boutonnet, B. Cojocaru, P.A. Primus, C.M. Teodorescu, C. Solans, M.S. Dominguez, Phys. Chem. Chem. Phys. 13 (2011) 17135–17145.
[49] C. Aubery, C. Solans, S. Prevost, M. Gradzielski, M.S. Dominguez, Langmuir 29 (2013) 1779–1789.
[50] G.Y. Liu, H.Y. Wang, G.Q. Liu, Z.Z. Yang, B. Jin, Q.C. Jiang, J. Power Sources 220 (2012) 84–88.
[51] Y.F. Tang, L. Yang, S.H. Fang, Z. Qiu, Electrochim. Acta 54 (2009) 6244–6249.
[52] Y.F. Tang, L. Yang, Z. Qiu, J.S. Huang, Electrochem. Commun. 10 (2008) 1513–1516.
[53] J.M. Feckl, K. Fominykh, M.D. Linger, D.F. Rohlfing, T. Bein, Angew. Chem. Int. Ed. 51 (2012) 7459–7463.
[54] J.Z. Chen, L. Yang, S.H. Fang, Y.F. Tang, Electrochim. Acta 55 (2010) 6596–6600.
[55] K. Zhu, Q. Wang, J.H. Kim, A.A. Pesaran, A.J. Frank, J. Phys. Chem. C 116 (2012) 11895–11899.
[56] X. Li, C. Lai, C.W. Xiao, X.P. Gao, J. Power Sources 56 (2011) 9152–9158.
[57] J. Haetge, P. Hartmann, K. Brezesinski, J. Janek, T. Brezesinski, Chem. Mater. 23 (2011) 4384–4393.
[58] B.Z. Li, Y. Wang, L. Xue, X.P. Li, W.S. Li, J. Power Sources 232 (2013) 12–16.